Design and analysis of low velocity impact on thermoplastic hat section with curvilinear profile

Kumresh K Gaur[*1,2], Mayank Dwivedi[2] and Naresh Bhatnagar[1]

[1]*Department of Mechanical Engineering, Indian Institute of Technology Delhi, Hauz Khas, 110016,*
New Delhi, India
[2]*Defence Research and Development Organization (DRDO), DRDO Bhawan, Rajaji Marg, 110011,*
New Delhi, India

Abstract. A hat section was designed and developed for maximum impact energy absorption and/or transmission under low velocity impact. Towards this, different hat sections, having material properties of thermoplastic, were modeled and investigated numerically using finite element analysis (FEA) in the range of 20-50 J impact energy. In the study it was experienced that the design configuration of hat section with curvilinear profile (HSCP) was excellent in energy attenuation capacity and for even distribution of maximum impact force around and along the hat section under low velocity impact loading. To validate the numerical findings, polypropylene copolymer (Co-PP) HSCP and low density polyethylene (LDPE) HSCP were developed and evaluated experimentally in the said impact energy range. A correlation was established between FEA and experimental test results, thereby, validating a numerical model to predict results for other thermoplastic materials under given range of impact energy. The LDPE HSCP exhibited better performance as compared to Co-PP HSCP in the said range of impact energy. The findings of this study will enable the engineers and technologists to design and develop low velocity impact resistance devices for various applications including devices to protect bone joints.

Keywords: hat section; curvilinear profile; low velocity impact; attenuation; numerical; experimental

1. Introduction

Structures having hat sections are known for absorbing and/or transmitting high energy on impact due to even distribution of stresses. David *et al.* (2005) have studied that the open segment of hat section undergoes premature buckling on impact since open segment tends to spread apart, kink and quickly lose shape upon impact. This point of view considered well in this research and therefore, a hat section was designed with curvilinear profile having an upper curved section at the top and curvilinear peripheral flat sections extending toward outer side of said hat section. The peripheral extension of the hat shaped portion stabilizes it during flexion on impact. This result in increased impact strength and energy absorption during impact, hence, reduced tendency to

---

∗Corresponding author, E-mail: gaur_87@yahoo.co.in

undergo sudden collapse. Plummer *et al.* (2004) have reported the thermoplastic (TP) materials are extensively being used for low velocity impact applications/personal safety appliances, many of these equipment and accessories are subjected to out of plane loading. The impact response of TPs play an important role in an efficient design of impact tolerant appliances which can minimize the energy transmitted to a person using them. Daiyan *et al.* (2010) have reported the ductile thermoplastic materials show a complex behaviour in impact loading involving large strains. Significant hardening of TP with increasing strain rates varies from one grade to another grade of same TP. However TPs have distinct advantages of light in weight, low cost, ease of processing and coupled with good mechanical properties. Therefore, the hat section with curvilinear profile (HSCP) made of thermoplastic opens a window for number of application in the field of automobile, healthcare, pedestrian safety and protective sports gears. Thermoplastic HSCP is likely to offer good attenuation of impact energy and prevention to the serious injuries to sports personals in field and elders at home or street due to fall. Spierings and Derler (2006) have reported the assessment of hip joint protectors and calculations related to fracture. The interpretation of low velocity impact (LVI) test involves a range of additional factors, occurring during the longer contact as compared to higher or ballistic impact. Ramakrishnan *et al.* (2013) have reported that dynamic histories and damage pattern are required to indicate the severity of event and provide an understanding of low velocity impact behavior of materials. Okayasu *et al.* (2014) have studied the importance of the loading behavior during testing. Computational simulation of low velocity impact loading of thermoplastic materials is of immense industrial interest. The constitutive models the industry typically uses for these materials today have small number when it comes to predicting multi-axial loading, unloading response and fracture. Several models for thermoplastic materials have been developed and tested in last several years. Ma *et al.* (2010), Drozdov *et al.* (2012) and Polanco-Loria *et al.* (2010) have reported that these models have described the key features of these materials, such as viscoelasticity, viscoplasticity, pressure-dependent yield stress, plastic dilatation and damage.

2. Materials

Commercially available TP materials namely polypropylene copolymer (Co-PP) (Haldia, Halene-P, M311T) and low density polyethylene (LDPE) (Reliance, 16MA400) were chosen for preparation of injection molded HSCP. Co-PP used was a heterophasic impact copolymer which was primarily suitable for injection molding process and combined excellent processability with high flow, low cycle time, good impact-stiffness balance with high toughness. Lei *et al.* (2013) have reported the presence of unstable crystalline part in polypropylene. This unstable crystalline part is absent in Co- PP. Co-PP doeLDPE used was an injection molding grade thermoplastic with high melt flow index that made it ideal for molding of intricate and complex shaped items with good mechanical properties. Selected properties of Co-PP and LDPE are given in Table 1. Co-PP and LDPE, offer excellent resistance to moisture and chemicals, such as, acid, alkalis and solvents as reported by Kaur *et al.* (2013).

3. Experimental

3.1 Preparation of HSCPs

Table 1 Properties of Co-PP and LDPE

Material	Melt flow index* (g/10 min)	Density at 23℃ (g/cm³)	Flexural modulus (MPa)	Tensile Strength at Yield (MPa)	Tensile Modulus (MPa)	Tensile Elongation at yield (%)	Vicat Softening Point (℃)
Co-PP	10	0.90	900	20	640	6	142
LDPE	30	0.92	140	10	102	40	84

*at 2.16 kg load & 190℃

(a) Front view of HSCP

(b) Side elevation view (left side) of HSCP   (c) Cross section taken along major axis A-A of HSCP
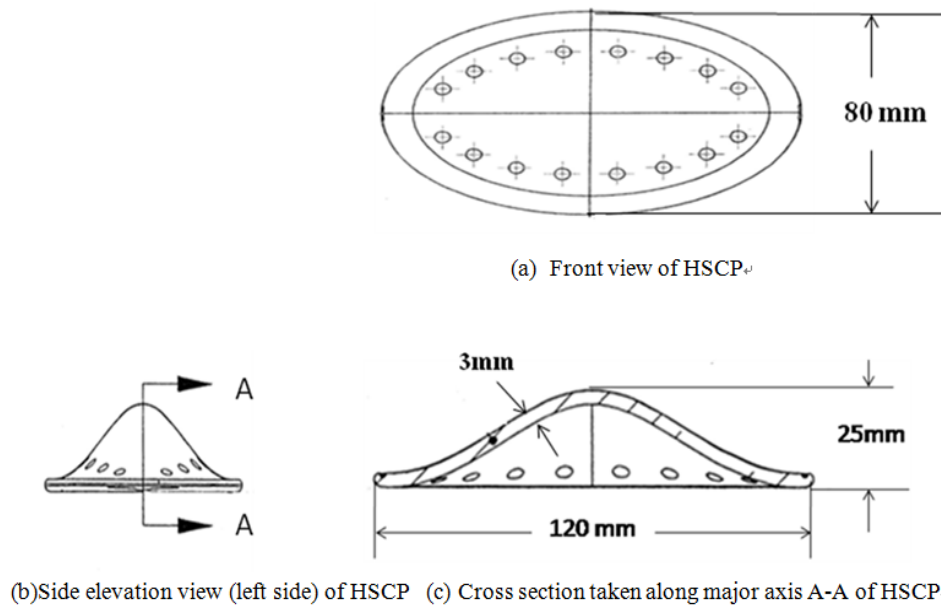
Fig. 1 Different view of hat section with curvilinear profile (HSCP)

Zakaria *et al.* (2010) have reported the geometry of the component, influences the impact resistance of the component significantly. Gardner *et al.* (2008) have reported that the shapes of most of the bone joints are in the form of ellipsoid with average diameter of 21±5 mm. Yurddaskal *et al.* (2016) have studied the effect of curvature for impact response. HSCPs were designed and developed accordingly. The shape of HSCP was elliptical with major axis and minor axis measuring 120 mm and 80 mm, respectively as shown in Fig. 1(a)-(c). The dimensions of projected hat section were having the height of 25 mm with major and minor axes measuring 70 mm and 30 mm, respectively. HSCPs were made for both the materials. The injection molding conditions were based on the standard ISO 1873-2:2007. Wu *et al.* (2014) have studied the injection moulding parameters such as injection speed, temperature, hold time and rheology to optimize the injection moulding process. The processing conditions for Co-PP; the mold and melt temperature were 45℃ & 240℃ and the maximum holding pressure was 55 MPa. For LDPE, the mold and melt temperature were 35℃ & 215℃ respectively and the maximum holding pressure was 45 MPa. The injection molding machine (Make: Battenfeld HM 40/210 S and Servo electric controlled) having maximum clamping force of 40 kN along with 25 mm diameter general purpose screw was used for molding of HSCPs.
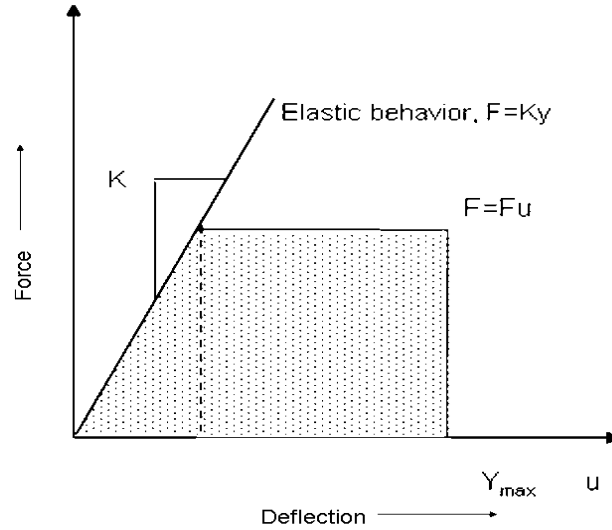
Fig. 2 Idealized elastic plastic behaviour

3.2 Analytical consideration of impact test

3.3.1 Elastic response of HSCPs under impact

Assuming that a HSCP is a simple elastic body, typically of a spring back in nature with a spring rate 'k'; struck by a mass, 'm'; having a weight, 'W', on which a load (Wg) strikes at velocity, 'V'. The impact force, 'F', experienced by HSCP and its equal and opposite reaction force slows the velocity of mass. Consequently, HSCP gets compressed by a maximum distance y_{max}. Liu *et al.* (2013) have reported the energy to be absorbed is the incoming kinetic energy plus the additional work done by the weight, 'W', and acting through HSCP deformation (y_{max}). The total energy absorbed is given by the following Eqs. (1)-(3).

Energy to be absorbed

$$E_k + Wy_{max} = \tfrac{1}{2}\tfrac{w}{g}V^2 + Wy_{max} \tag{1}$$

Where E_k is the kinetic energy of a falling weight and W is the weight of falling mass.
Equating energy absorbed and the work of elastic deformation-

$$E_k + Wy_{max} = \tfrac{1}{2}ky_{max^2} \tag{2}$$

Or by rearranging

$$y_{max} = \tfrac{w}{k}\left(1+\sqrt{1+\tfrac{2kE_k}{W^2}}\right) = y_{st}\left(1+\sqrt{1+\tfrac{2E_k}{Wy_{st}}}\right) \tag{3}$$

Where, Y_{st} is the static deflection of the HSCP under the weight, 'W'. Since the displacement and load are proportional to each other, the effective force experienced by HSCP, during impact, is the product of the dynamic amplification and the weight. Wright (2012) has reported that a load suddenly applied from rest produces twice the stress and twice the displacement as the same load applied gradually.

3.3.2 Plastic response of the HSCP under impact

In elastic collisions, energy is lost and none goes into yielding or frictional resistance. In general, the designs which are rugged enough to withstand large collisions elastically are heavy. In elastic idealization, the deformation behaviour is linear-the force needed to deform or deflect the test specimen (HSCP) is proportional to the displacement. In practice the force variation is linear only up to the onset of yielding or crushing, which occurs without further increase in resistance. The limiting load may be taken as the load at the onset of yielding for axially loaded specimen or the load require to produce onset of plastic deformation in test specimen.

Fig. 2 shows idealized elastic plastic behaviour in general. The hashed area represents the energy absorbed by a HSCP undergoing yielding. Ravid and Bodner (1983) have studied the displacement increases linearly up to the limit load, F_u after which the specimen deforms without additional force. The energy integral is simply the area under the curve as given in Eq. (4).

$$E_p = \int_O^y Fdu = F_u y_{max} - \frac{F_u^2}{2k} \tag{4}$$

Equating the kinetic energy of impact and the strain energy gives HSCP deformation as given in Eq. (5).

$$y_{max} = \frac{Ek + \frac{F_u^2}{2k}}{F_u}, \text{ where } k = \text{Amount of weight required to deflect a specimen} \tag{5}$$

The displacement, y_{max}, is limited in practice by the ability of HSCP to absorb plastic deformation without becoming unstable.

The ratio of the total deformation to the elastic deformation is conventionally called the 'ductility factor,' μ. The ductility factor relates elastic capacity of HSCP and impact load in a useful way, using a simple energy balance. Suppose HSCP is subjected to an external load, F, equating the work done by impact force, Fy_{max}, to energy absorbed by HSCP as shown in the Fig. 2 which provides the following energy balance as given in Eq. (6).

$$Ey_{max} = \tfrac{1}{2} F_u y_u + F_u\left(y_{max} - y_u\right) or \frac{F_u}{F} = \frac{2\mu}{2\mu-1}, \text{ Where: } \mu = \text{ the ductility factor}, \frac{y_{max}}{y_u} \tag{6}$$

The relationship expresses the required capacity of HSCP for elastic deformation; F_u is the anticipated load to which certain degree of damage is to be tolerated.

As per empirical equation, ductility factor exceeding 10 is associated with very heavy damage whereas; the ductility factor below 5 produces tolerable damage which will probably allow HSCP to be used again.

3.3 Numerical simulation and finite element model implementation

Sezer *et al.* (2007) have reported the FEA is to divide the body into finite elements, often just called elements. It is designed to contain the structural properties and the material which specifies how the structure will react under specific loading conditions. Duan *et al.* (2003), Dean *et al.* (2003), Kharazan *et al.* (2015) and Aghaei *et al.* (2015) have studied that the analysis of multiaxial impact behaviour and finite element method are important for simulation and prediction of deformation of polymers and composites under low velocity impact. Zouambi *et al.* (2014) have modeled the bone joints for computational analysis and predicted the stress behavior. In this study, for numerical analysis, a commercially available finite element analysis code ANSYS Ver.13 (Explicit STR) was used to simulate the falling conditions of a drop weight for different descend

heights. The software was fully integrated into the unified Ansys Workbench environment. The equations solved by this explicit dynamic analysis code expressed the conservation of mass, momentum and energy in Lagrange coordinates. These, together with a material model and a set of initial boundary conditions, defined the complete solution of the problem. In Lagrange formulations, the mesh moves and distorts with the material model, so conservation of mass is automatically satisfied. The density at any time can be determined from the current volume of the zone and its initial mass as given in Eq. (7).

$$\frac{\rho_o V_o}{V} = \frac{m}{V} \tag{7}$$

Where ρ_o=Initial density of the material in each element
V_o=Initial volume of the material in each element
V=Volume of the element at the computational time and m=Mass
The partial differential equations, which express the conservation of momentum, relate the acceleration to the stress tensor by the following set of Eqs. (8)-(10)

$$\rho\ddot{x} = b_x + \frac{\partial\sigma_{xx}}{\partial x} + \frac{\partial\sigma_{xy}}{\partial y} + \frac{\partial\sigma_{xz}}{\partial z} \tag{8}$$

$$\rho\ddot{y} = b_y + \frac{\partial\sigma_{yx}}{\partial x} + \frac{\partial\sigma_{yy}}{\partial y} + \frac{\partial\sigma_{yz}}{\partial z} \tag{9}$$

$$\rho\ddot{z} = b_z + \frac{\partial\sigma_{zx}}{\partial x} + \frac{\partial\sigma_{zy}}{\partial y} + \frac{\partial\sigma_{zz}}{\partial z} \tag{10}$$

Where ρ=Density of the element at the computation time obtained from previous equation $\ddot{x}, \ddot{y}, \ddot{z}$ = Nodal acceleration in x, y and z directions

b_x, b_y, b_z=Body forces acting in x, y, and z directions

σ_{xx}, σ_{yy}, σ_{zz}, σ_{xy}, σ_{xz}, σ_{yx}, σ_{yz}, σ_{zx}, σ_{zy} are the stresses in x, y and z co-ordinates and conservation of energy is expressed via Eq. (11).

$$\dot{e} = \frac{1}{\rho}\left(\sigma_{xx}\dot{\varepsilon}_{xx} + \sigma_{yy}\dot{\varepsilon}_{yy} + \sigma_{zz}\dot{\varepsilon}_{zz} + 2\sigma_{xy}\dot{\varepsilon}_{xy} + 2\sigma_{yz}\dot{\varepsilon}_{yz} + 2\sigma_{zx}\dot{\varepsilon}_{zx}\right) \tag{11}$$

Where $\dot{e}$ Rate of change of energy, $\dot{\varepsilon}_{xx}\dot{\varepsilon}_{yy}\dot{\varepsilon}_{zz}$=Rate of change of strain in x, y and z directions (change of internal energy is consumed in straining the elements)

For each time step, these equations are solved explicitly for each finite element in the model, based on input values at the end of the previous time step. The Explicit Dynamics solver uses a central difference time integration scheme (Leapfrog method). After forces have been computed at the nodes (resulting from internal stress, contact, or boundary conditions), the nodal accelerations are derived by dividing the force by mass as given in Eq. (12).

$$\ddot{X}_i = \frac{F_i}{m} + b_i \tag{12}$$

Where x_i are the components of nodal acceleration (i=1, 2, 3), F_i are the forces acting on the nodes, b_i are the components of body acceleration and m is the mass of the node. With the accelerations at time $n-\frac{1}{2}$ determined, the velocities at time $n+\frac{1}{2}$ are found from Eq. (13).

$$\dot{X}_i^{n+1/2} = \dot{X}_i^{n-1/2} + \ddot{X}_i^{n}\Delta t^n \tag{13}$$

(a) FEA models of HSCP   (b) Simulated effective deformation
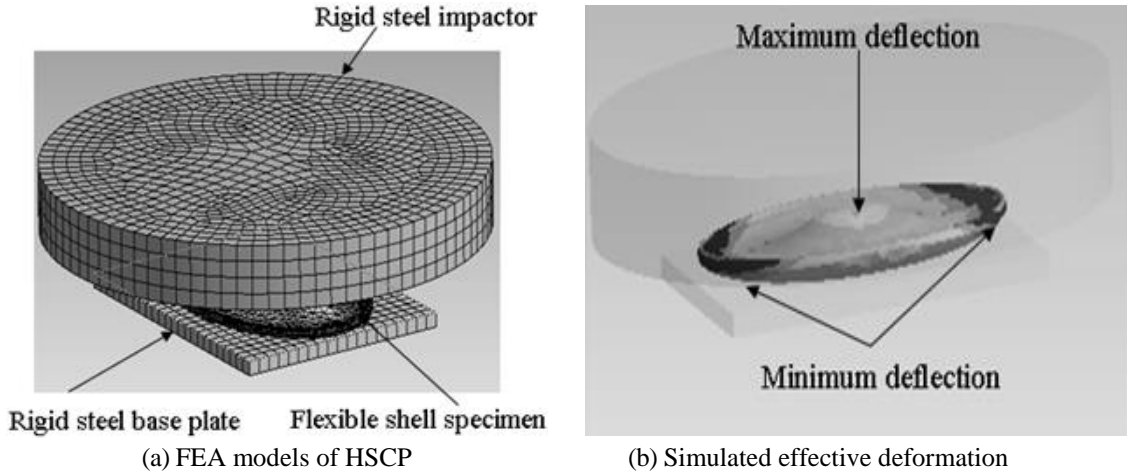
Fig. 3 FEA models of HSCP

Finally the positions are updated to time $n+1$ by integrating the velocities through Eq. (14).

$$x_i^{n+1} = x_i^n + \dot{x}_i^{n+1/2} + \Delta t^{n+1/2} \qquad (14)$$

By using this method for time integration for nonlinear problems, the equations became uncoupled and could be solved directly (explicitly). There was no requirement for iteration during time integration. No convergence checks were needed since the equations were uncoupled and no inversion of the stiffness matrix was required.

Courant *et al.* (1967) have studied to ensure stability and accuracy of the solution, the size of the time step used in explicit time integration is limited by the Courant-Friedrichs-Levy condition. This condition implies that the time step be limited such that a disturbance (stress wave) cannot travel further than the smallest characteristic element dimension in the mesh, in a single time step. Thus the time step criteria for solution stability is given by Eq. (15).

$$\Delta t \le f * \left[\frac{h}{c} \right]_{min} \qquad (15)$$

Where Δt is the time increment, f is the stability time step factor h is the characteristic dimension of an element and c is the local material sound speed in an element. With reference to above analysis, settings for this study were finalized by keeping maximum number of cycle 1e+7 and end time 7e-5.

For meshing the geometry of HSCP model, different meshing methods available in ANSYS were tried to assess their effect on mesh density and size. The model was solved in explicit dynamics that examines the time step resulting from different mesh methods. Finally, HSCP geometry meshed by hexahedral mesh was swept through the thickness of the model. The model used in this study contains 9859 nodes and 19015 elements.

Michael (2004) reported threshold value of impact force required for bone hip joints injuries due to fall. Based on these two velocities, were preferred i.e., 2.8 ms^{-1} and 4.2 ms^{-1}. These velocities were used to simulate the falling conditions of a drop weight impact on HSCP. The velocity was increased incrementally from 2.8 to 4.2 ms^{-1} to assess the capability of HSCPs to sustained maximum impact force before failure. An impactor of effective mass of 5.6 kg was

allowed to strike the Co-PP HSCP and LDPE HSCP with both the velocities. Fig. 3 shows FEA models of HSCP for the velocity undergoing drop weight impact with a flat rigid surface. The stiffness behaviour of HSCP was defined as flexible which allowed it to press crush and spring back. The materials used were Co-PP and LDPE which have linear elastic stress strain relationship at low strains or up to the yield stress followed by nonlinear plastic deformation for large strains. The linear elastic unit was described by the Young's modulus (E), Poisson's ratio (v) and proportionality limit or yield stress. The nonlinear plastic deformation was described by stain hardening curve, as obtained from the plot of true tensile stress vs true tensile plastic strain. The impactor and base plate stiffness behaviour was defined as a rigid body and material properties assigned were of structural steel which was available in explicit materials library. The contact between the impactor and HSCP were defined by contact algorithm available in ANYSIS/Explicit. Balasubramani *et al.* (2013) have reported the contact force can be defined as the response force of samples against the impactor. The impactor was allowed to move in vertical downward direction and base plate was defined as rigidly fixed support. Duan *et al.* (2002) have studied the numerical simulation of the impact response of thermoplastic components under mechanical loading as a verification case for the material models, mainly focusing on the loading up to maximum load.

3.4 Impact testing

An experimental study was carried in order to compare and validate the numerical results as obtained for energy attenuation capacity of injection molded HSCPs made of Co-PP and LDPE. In experimental study, low velocity impact (LVI) and moderate velocity impact (MVI) tests were performed. Safri *et al.* (2014) have reported the impactor weight, shape, elastic properties and incident angles are important parameters required to be considered in impact analysis. Further, Flores-Johnson and Li (2011) have studied the penetration force depends on the geometry of the impactor and the density of the polymeric material. Accordingly in this LVI test, the stainless steel flat impactor of effective mass 5.6 Kg was allowed to drop in vertical direction from a height of 0.4 m and to strike the HSCP, the ensuing impact velocity and energy accomplish on HSCP was 2.8 ms^{-1}, and 21.9 J respectively. In MVI test, the same impactor was allowed to drop in vertical direction from a height of 0.9 m and to strike the HSCP, the ensuing impact velocity and energy accomplish on HSCP was 4.2 ms^{-1} and 49.4 J respectively using a Dynatup 9250 HV model (which is a specially designed machine of Instron for vertical drop weight impact test). The machine included high performance test frame, high bandwidth digital signal processing electronics, self-identifying load cells, and impulse control and data acquisition software. The impact energies were measured with the load cell, where, the peak impact value was determined automatically by the in-built analysis software. For each experimental study, a total of 8200 data points were collected during impact event by the data acquisition system, and subsequently they were converted in to impact force vs time, impact force vs deflection and absorbed energy vs time behavior.

4. Results and discussion

A series of drop tests were performed on HSCP at low and moderate impact energy level, for comparison of experimental results with numerical analysis. Effect of impact velocity, stress triaxiality and damage were assessed. Results were discussed in order to corroborate the

Table 2 Results of force vs deflection behavior

Mode of study	Deflection in Co-PP HSCP		Deflection in LDPE HSCP	
	At LVI (2.8ms^{-1}) (impacted energy 21.9 J)	At MVI (4.2ms^{-1}) (impacted energy 49.4 J)	At LVI(2.8 ms^{-1}) (impacted energy 21.9 J)	At MVI (4.2 ms^{-1}) (impacted energy 49.4 J)
Numerical Analysis	12.8 mm	19.1 mm	7.3 mm	12.5 mm
Experimental Analysis	11.0 mm	17.4 mm	6.9.0 mm	11.3 mm

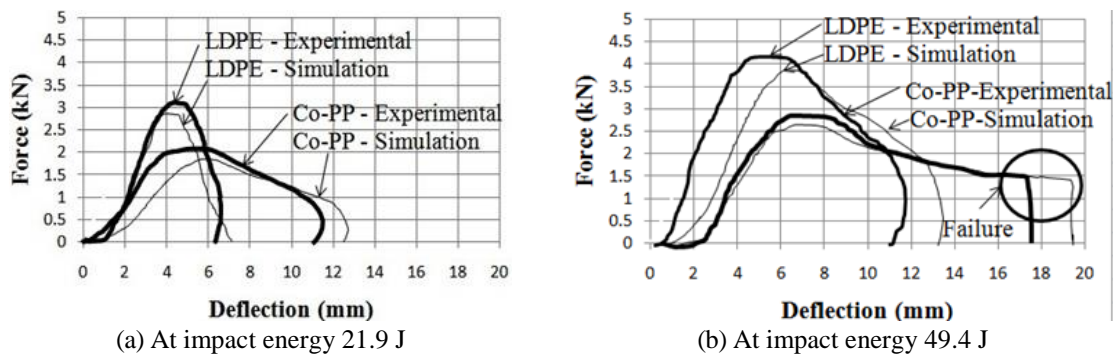(a) At impact energy 21.9 J   (b) At impact energy 49.4 J

Fig. 4 Force vs deflection behavior of Co-PP and LDPE HSCP

Table 3 Results of absorbed energy vs time behavior

Mode of study	Energy absorbed by Co-PP HSCP		Energy absorbed by LDPE HSCP	
	At LVI (2.8ms^{-1}) (impacted energy 21.9 J)	At MVI (4.2ms^{-1}) (impacted energy 49.4 J)	At LVI(2.8 ms^{-1}) (impacted energy 21.9 J)	At MVI (4.2 ms^{-1}) (impacted energy 49.4 J)
Numerical Analysis	11.0 J	22.5 J	12.5 J	29.0 J
Experimental Analysis	12.5 J	25.0 J	14.0 J	31.0 J

sustainability of HSCPs to be used as safety gears to prevent injuries and to assess the limit of HSCPs to sustain impact energy before failure.

4.1 Force vs deflection behavior

The low velocity (2.8 ms^{-1}) and moderate velocity (4.2 ms^{-1}) signify impact energies of 21.9J and 49.4 J, respectively. The results of FEA simulation and experiments for LVI and MVI in cases of LDPE HSCP and Co-PP HSCP are tabulated in Table 2.

The plots of these values for instant comparison at different deflections are given in Fig. 4(a)-(b). It was also evaluated from plots that FEA values are in close comparison with experimental values, thus, validating the numerical findings for force Vs deflection behavior.

From Fig. 4(b), it was also observed that Co-PP HSCP, at 49.4 J impact energy elongated and stretched along the deformation axis with small reduction in impact force and finally exhibited an unexpected sudden drop in impact force. This was attributed to the catastrophic damage and eventually a fracture of the Co-PP HSCP. Whereas, no failure behaviour was observed for LDPE HSCP either in experiments or in FE based numerical analysis at impact energy of 49.4 J. This was
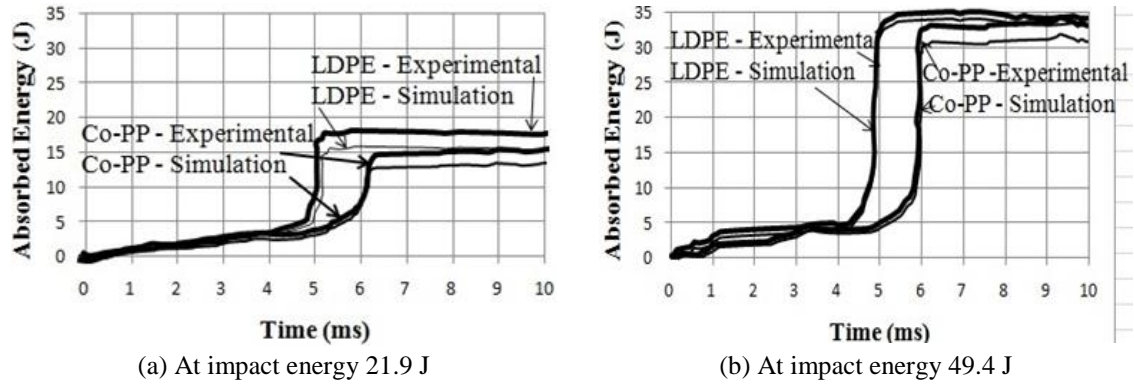
(a) At impact energy 21.9 J   (b) At impact energy 49.4 J

Fig. 5 Absorbed energy vs time behaviour of Co-PP and LDPE HSCP

Table 4 Results of force vs time behavior

Mode of study	Impact force delivered on PP HSCP		Impact force delivered on LDPE HSCP	
	At LVI (2.8ms^{-1}) (impacted energy 21.9 J)	At MVI (4.2ms^{-1}) (impacted energy 49.4 J)	At LVI(2.8 ms^{-1}) (impacted energy 21.9 J)	At MVI (4.2 ms^{-1}) (impacted energy 49.4 J)
Numerical Analysis	1.9 kN	2.7 kN	2.8 kN	4.0 kN
Experimental Analysis	2.1 kN	3.0 kN	3.1 kN	4.5 kN

(a) At impact energy 21.9 J   (b) At impact energy 49.4 J

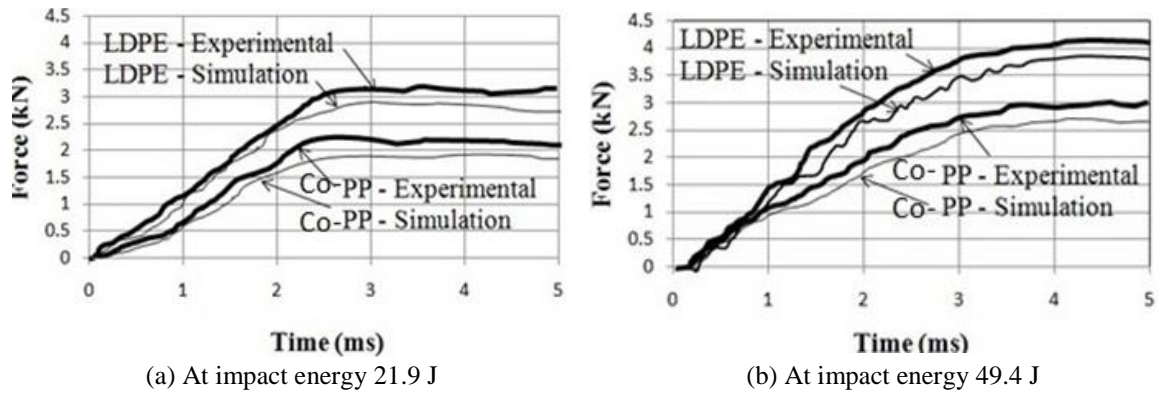Fig. 6 Force vs time behavior of Co-PP and LDPE HSCP

attributed to the inherent high impact resistance of the LDPE at high loading rates.

4.2 Absorbed energy vs time behavior

Absorbed energy vs time curves are given in Fig. 5(a)-(b). In this study HSCPs of Co-PP and LDPE were analyzed, through FEA and experimentally, at 21.9 J and 49.4 J impact energies. The results of the study are tabulated in Table 3.

From curves it was noticed that a good correlation existed between the numerical and experimental results with a little difference in energy absorbing capacity of both the materials. The curves of Fig. 5(a)-(b) also signifying that the smaller impact time delivered more impact force

(a) Front surface of Co-PP HSCP at impact energy 21.9 J

(b) Bottom surface of Co-PP HSCP at impact energy 21.9 J

(c) Front surface of LDPE HSCP at impact energy 21.9 J

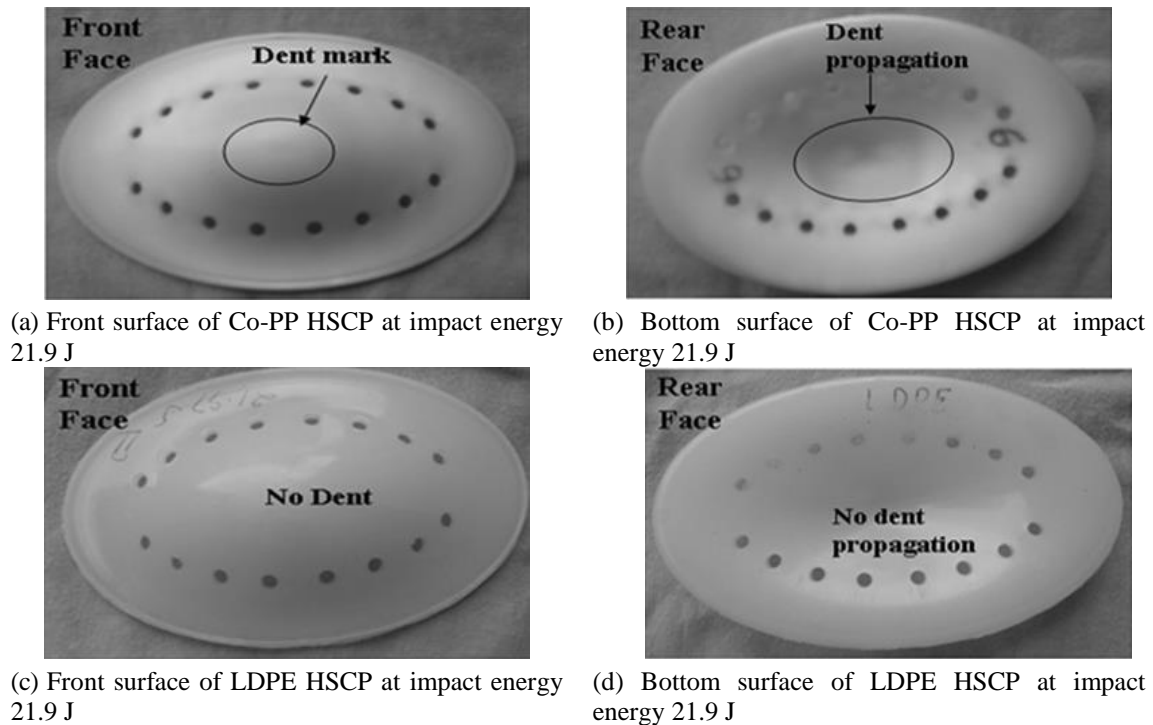(d) Bottom surface of LDPE HSCP at impact energy 21.9 J

Fig. 7 Impact damage behavior of Co-PP and LDPE HSCP

resulting in higher impact energy absorption and superior spring back property of the LDPE HSCP compared to Co-PP HSCP.

4.3 Force vs time behavior

The force vs time behavior results of FEA simulation and experiments for LVI and MVI in the cases of LDPE HSCP and PP HSCP are tabulated in Table 4.

Force vs time graphs are shown in Figs. 6(a)-(b) illustrated that the impact force increases with increase in impact energy. From the curves it is observed that LDPE HSCP has higher force carrying capacity compare to Co-PP HSCP at both the impacted energies. FEA results are in close comparison with the experimental results for all impact energies. Thus testifying the validating of numerical model for force vs time behavior.

From above results, it is observed that the small variation existed between numerical and experimental results. The reason for this might be attributed to the limitations of numerical model used in this study. The model exercised in this study was based on a number of assumptions and simplifications. The validity and correctness of these models depend on mechanical loading, geometry of the part, material characteristics, mechanical properties during experiments and data used in FEA simulations. There is an always a gap in values of theoretically exerted load and actually experienced load by test specimen. Similar, the multiaxial distribution and resulting stresses, occur in actual experiment, are difficult to simulate in FEA simulation. However, in this study, due to axis symmetric body in the form of HSCP produces close compromise in the value of FEA simulation and experimental data. Further, this model also has not taken into account the

(a) Front surface of Co-PP HSCP at impact energy 49.4 J

(b) Bottom surface of Co-PP HSCP at impact energy 49.4 J

(c) Front surface of LDPE HSCP at impact energy 49.4 J

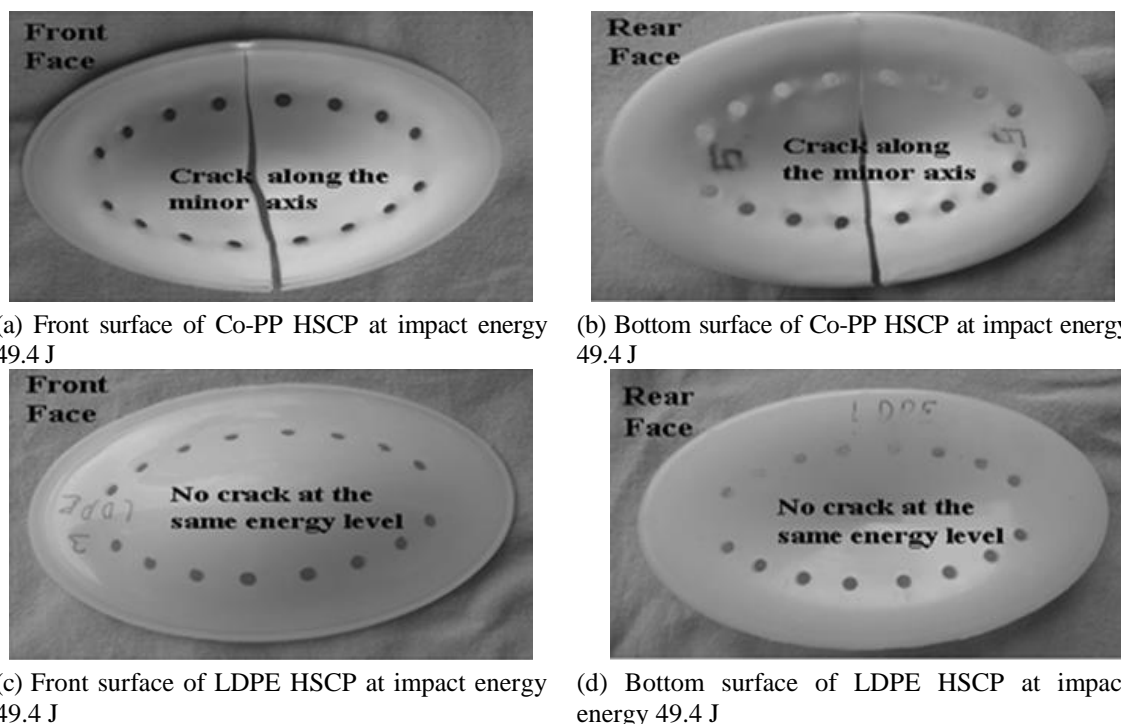(d) Bottom surface of LDPE HSCP at impact energy 49.4 J

Fig. 8 Impact damage behavior of Co-PP and LDPE HSCP

anisotropy and the heterogeneity of injection molded HSCP. The anisotropy was due to orientation of thermoplastic chains and crystallites, which was induced by the molding process. The heterogeneity was the result of the spatial variation in the thermo-mechanical conditions during molding, resulting in a variation in properties through the cross-section of the HSCP, and along the flow path.

4.4 Impact damage

Fig. 7 and 8 illustrate the top and bottom surfaces of the impacted Co-PP and LDPE HSCPs, respectively. In Fig. 7 (a)-(b), a dent was seen on front face and also its propagation on the rear face of the Co-PP HSCP. Whereas, no occurrence of dent and its propagation were observed for LDPE HSCP in Fig. 7(c)-(d). Therefore, it was clear that LDPE HSCP had good impact resistance as compared to Co-PP HSCP at impact energy of 21.9 J. The size of the impact damage zone increased with increase in velocity of impact and the damage pattern was of the same shape around the point of impact in Co-PP HSCP. This zone was not observed in LDPE HSCP even at moderate impact energy. Co-PP HSCP exhibited larger deformation compared to LDPE HSCP due to its poor interfacial adhesion between Co-PP HSCP macromolecules.

The inclusive damage of the Co-PP HSCP was absorbed along the minor axis, whereas no occurrence of damage in LDPE HSCP was absorbed at 49.4 J impact energy test as shown in Fig. 8(a)-(d). Consequently, LDPE HSCP exhibited no damage as compared to Co-PP HSCP due to its branching in linear molecular chains and this exhibited better resistance to impact at high loads and established its suitability for impact applications.

A higher impact damage resistance of the LDPE HSCP, compared to Co-PP HSCP, was observed due its better interfacial adhesion among polymeric chains and semicrystalline nature. Furthermore, long molecular chain and high molecular weight of LDPE significantly enhanced the absorption of impact energy compared to Co-PP which has shorter molecular chains and lower molecular weight.

5. Conclusions

In this study, the numerical model of a curvilinear hat profile made out of two different thermoplastics (CoPP and LDPE) was validated experimentally for a low velocity impact. This numerical model facilitated a close prediction of energy absorption behaviour of both the thermoplastics under low velocity impact up to 49.4 J. The study also revealed that the low velocity damage resistance of curvilinear hat profile of LDPE is found to be superior to CoPP. This numerical model indicates its suitability for design and analysis of range of thermoplastic products such as automotive parts, sports/recreational goods, medical devices etc., which experience low velocity impacts.

References

Aghaei, M., Forouzan, M.R., Nikforouz, M. and Shahabi, E. (2015), "A study on different failure criteria to predict damage in glass/polyester composite beams under low velocity impact", *Steel Compos. Struct.*, **5**(18), 1291-1303.

Balasubramani,V., Rajinder B.S. and Vasudevan, R. (2013), "Numerical analysis of low velocity impact on laminated composite plates", *Proc. Eng.*, **64**, 1089-1098.

Courant, R., Friedrichs, K. and Lewy, H. (1967), "The partial difference equations of mathematical physics", *IBM*, 215-234.

Daiyan, H., Andreassen, E., Grytten, F., Lyngstad, O.V., Luksepp, T. and Osnes, H. (2010), "Low-velocity impact response of injection-moulded polypropylene plates-part 1: Effects of plate thickness, impact velocity and temperature", *Polym. Test*, **29**(6), 648-657.

Dean, G. and Wright, L. (2003), "An evaluation of the use of finite element analysis for predicting the deformation of plastics under impact loading", *Polym. Test.*, **22**(6), 625-631.

Drozdov, A.D., Al-Mulla, A. and Gupta, R.K. (2012), "Structure-property relations for polymer melts: Comparison of linear low-density polyethylene and isotactic polypropylene", *Adv. Mater. Res.*, **4**(1), 245-268.

Duan, Y., Saigal, A., Greif, R. and Zimmerman, M.A. (2002), "Analysis of multiaxial impact behavior of polymers", *Poly. Eng. Sci.*, **42**(2), 395-402.

Flores-Johnson, E.A. and Li, Q.M. (2011), "Low velocity impact on polymeric foams", *J. Cell. Plast.*, **47**(1), 45-63.

Gardner, M.J., Robertson, W.J., Boraiah, S., Barker, J.U. and Lorich, D.G. (2008), "Anatomy of the greater trochanteric 'bald spot: A potential portal for abductor sparing femoral nailing", *Clin. Ortho. Relat. Res.*, **466**(9), 2196-2396.

Heatherington, D., Glasgow, S. and Bruce Lyons, B. (2005), *Vehicle Bumper Beam*, US 20050285416 A1.

Kaur, I., Gupta, N. and Kumari, V. (2013), "Functionalization of polyethylene by graft copolymerization for separation processes", *Adv. Mater. Res.*, **1**(2), 15-36.

Kharazan, M., Sadr, M.H. and Kiani, M. (2014), "Delamination growth analysis in composite laminates subjected to low velocity impact", *Steel Compos. Struct.*, **4**(17), 387-403.

Caihong, L.C., Wu, S., Xu, R., Xu, Y. and Peng, X. (2013), "A study of plastic plateau disappearance in stress-strain curve of annealed polypropylene films during stretching", *Adv. Mater. Res.*, **2**(2), 111-118.

Liu, B., Villavicencio, R. and Guedes, S. (2013), "Experimental and numerical plastic response and failure of pre-notched transversely impacted beams", *Mech. Sci.*, **77**, 314-332.

Ma, Q., Su, X., Lin, Z., Lasecki, J. and Lai, X. (2010), "A constitutive model for the nonlinear viscoplastic behavior of thermoplastic olefin", *Polym. Compos.*, **31**(4), 587-595.

Michael, M. (2004), *Hip Protector System*, US20040049827 A1.

Okayasu, M., Yano, K. and Shiraishi, T. (2014), "Effects of loading conditions on the fatigue failure characteristics in a polycarbonate", *Adv. Mater. Res.*, **3**(3), 163-174.

Plummer, C.J.G. (2004), "Micro deformation and fracture in bulk polyolefins", *Adv. Poly. Sci.*, **169**, 75-120.

Polanco-Loria, M., Clausen, A.H., Berstad, T. and Hopperstad, O.S. (2010), "Constitutive model for thermoplastics with structural applications", *J. Imp. Eng.*, **37**(12), 1207-1219.

Ramakrishnan, K.R. and Shankar, K. (2013), "Experimental and numerical analysis of low velocity impact on plastic laminates", *J. FFEMS*, **36**(11), 1153-1163.

Ravid, M. and Bodner, S.R. (1983), "Dynamics perforation of viscoplastic plates by rigid projectiles", *Eng. Sci.*, **21**(6), 577-590.

Safri, S.N.A., Sultan, M.T.H., Yidris, N. and Mustapha, F. (2014), "Low velocity and high velocity impact test on composite materials-a review", *J. IJES*, **3**, 50-60.

Sezer, H. and Atamturktur, M.S. (2007), "Thesis defence structural assessment of guastavino domes", 10-12.

Spierings, A.B. and Derler, S. (2006), "Assessment of hip protectors and corresponding hip fracture risk using stress calculation in the femoral neck", *Med. Eng. Phys.*, **28**(6), 550-559.

Wright, P.E. (2012), *Introduction to Structural Impact*, PHD Course S164, Meadow Estates Drive, Fairfax, U.S.A.

Wu, C.L. and Lin, C.C. (2014), "Study molded part quality of plastic injection process by melt viscosity evaluation", *Adv. Mater. Res.*, **2**(3), 327-339.

Yurddaskal, M. and Baba, B.O. (2016), "The effect of curvature on the impact response of foam-based sandwich composite panels", *Steel Compos. Struct.*, **5**(20), 983-997.

Zakaria, M., Keith, W., Kambiz, K. and James, N. (2010), "Low velocity impact behavior of glass filled fiber-reinforced thermoplastic engine components", *Mater. Art.*, **3**(4), 2463-2473.

Zouambi, L., Serier, B. and Benamara, N. (2014), "Effect of cavity-defects interaction on the mechanical behaviour of the bone cement", *Adv. Mater. Res.*, **1**(3), 35-45.

CC